

Article

Controlling O Reactivity in Synthetic Analogues of [NiFeS]- and [NiFeSe]-Hydrogenase Active Sites

Xuemei Yang, Lindy C. Elrod, Trung Le, Valeria S. Vega, Haley Naumann, Yohannes Rezenom, Joseph H Reibenspies, Michael B. Hall, and Marcetta Y. Darensbourg

J. Am. Chem. Soc., **Just Accepted Manuscript** • DOI: 10.1021/jacs.9b07448 • Publication Date (Web): 29 Aug 2019

Downloaded from pubs.acs.org on August 30, 2019

Just Accepted

“Just Accepted” manuscripts have been peer-reviewed and accepted for publication. They are posted online prior to technical editing, formatting for publication and author proofing. The American Chemical Society provides “Just Accepted” as a service to the research community to expedite the dissemination of scientific material as soon as possible after acceptance. “Just Accepted” manuscripts appear in full in PDF format accompanied by an HTML abstract. “Just Accepted” manuscripts have been fully peer reviewed, but should not be considered the official version of record. They are citable by the Digital Object Identifier (DOI®). “Just Accepted” is an optional service offered to authors. Therefore, the “Just Accepted” Web site may not include all articles that will be published in the journal. After a manuscript is technically edited and formatted, it will be removed from the “Just Accepted” Web site and published as an ASAP article. Note that technical editing may introduce minor changes to the manuscript text and/or graphics which could affect content, and all legal disclaimers and ethical guidelines that apply to the journal pertain. ACS cannot be held responsible for errors or consequences arising from the use of information contained in these “Just Accepted” manuscripts.

Controlling O₂ Reactivity in Synthetic Analogues of [NiFeS]- and [NiFeSe]-Hydrogenase Active Sites

Xuemei Yang^a, Lindy C. Elrod^a, Trung Le^a, Valeria S. Vega^a, Haley Naumann^a,
Yohannes Rezenom^a, Joseph H. Reibenspies^a, Michael B. Hall^a, and Marcetta Y. Darensbourg^{a*}
^a Texas A&M University, Department of Chemistry, College Station, TX 77843, USA
Fax: (internat.) +1-979-845-0158
E-mail: marcetta@mail.chem.tamu.edu

Abstract:

Strategies for limiting, or reversing, the degradation of air-sensitive, base metal catalysts for the hydrogen evolution/oxidation reaction on contact with adventitious O₂ are guided by Nature's design of hydrogenase active sites. The affinity of oxygen for sulfur and selenium, in [NiFeS]- and [NiFeSe]-H₂ase, yields oxygenated chalcogens under aerobic conditions, and delays irreversible oxygen damage at the metals by maintaining the NiFe core structures. To identify the controlling features of S-site oxygen uptake, related Ni(μ-E_{PhX})(μ-S'_{N2})Fe (E = S or Se, Fe = (η⁵-C₅H₅)Fe^{II}(CO)) complexes were electronically tuned by the para substituent on μ-E_{PhX} (X = CF₃, Cl, H, OMe, NMe₂), and compared in aspects of communication between Ni and Fe. Both single and double O-atom uptake at the chalcogens led to the conversion of the 4-membered core, Ni(μ-E_{PhX})(μ-S'_{N2})Fe, to a 5-membered Ni-O-E-Fe-S', where an O atom inserts between E and Ni. In the E = S, X = NMe₂ case, the 2-oxygen uptake complex was isolated and characterized as the sulfinato species with the second O of the O₂S_{Ph-NMe₂} unit pointing out of the 5-membered Ni-O-S-Fe-S' ring. Qualitative rates of reaction and ratios of oxygen-uptake products correlate with Hammett parameters of the X substituent on E_{PhX}. DFT computational results support the observed remote effects on the NiFe core reactivity; the more electron-rich sulfurs are more O₂ responsive in the S_{PhX} series; the selenium analogues were even more reactive with O₂. Mass spectral analysis of the sulfinato products using a mixture of ¹⁸O₂/¹⁶O₂ suggests a concerted mechanism in O₂ addition. Deoxygenation, by reduction or O-atom abstraction reagents, occurs for the 1-O addition complexes, while the 2-O, sulfinato, analogues are inert. The abstraction of oxygen from the 1-O, sulfenato species, is related to oxygen repair in soluble, NAD⁺-reducing [NiFe]-H₂ase. (Horch, M., Lauterbach, L., et al., *J. Am. Chem. Soc.* **2015**, *137*, 2555-2564.)

Introduction

The deleterious effect of O₂ comprises a major challenge in technological development of molecular catalysts for H⁺ reduction based on abundant transition metals, needed for sustainable electron conversion to H₂.¹⁻² Oxygen as a poison is also well known to the organisms dependent on Hydrogenase enzymes for H₂ production for its use as an energy vector in many biological pathways.³ Evolution over billions of years has developed various strategies for protection from O₂ as a competing, degrading substrate for Hydrogenase enzymes as well as possible self-repair mechanisms. Among the different types of Hydrogenases, only the [NiFe]-H₂ases provide examples of the capability to operate in the presence of O₂; These are examples of oxygen tolerance.

1
2
3 At least three natural strategies have emerged to protect [NiFe]-H₂ases' active sites from oxygen
4 exposure: (i) a narrow hydrophobic gas channel that hinders diffusion of the bulkier O₂ into the
5 protein-enclosed active site;⁴⁻⁵ (ii) the presence of an unusual [4Fe-3S] subunit located at the
6 proximal cluster of the O₂-tolerant membrane-bound [NiFe]- H₂ase such as that of MBH from the
7 hyperthermophilic bacterium *Aquifex aeolicus* and *Ralstonia eutropha*, which provides “an
8 electron-rich environment for O₂ detoxification”;⁶⁻¹¹ and (iii) the change of a terminal cysteine
9 into selenocysteine in the O₂-resistant [NiFeSe]-H₂ases.¹²

10
11
12 Known to be superior to the all-sulfur analogue, the [NiFeSe]-H₂ase subfamily shows
13 higher activity in HER; reduced inhibition by the product H₂; and, when damaged by adventitious
14 O₂, a more rapid recovery.¹³⁻¹⁵ The last feature is likely the greatest contributor to its reputation
15 for O₂ tolerance. The overall protein as well as the active sites of [NiFeS]- and [NiFeSe]-H₂ase are
16 structurally analogous. In the same position as a terminal cysteine sulfur in the former that acts as
17 a proton shuttle to the hydride-loaded NiFe unit, the selenocysteine appears to be poised for the
18 same function in [NiFeSe]-H₂ase.¹⁶ Although SeR⁻ is a poorer Brønsted-Lowry base than SR⁻,
19 and expected to be less prone to proton binding, its larger size renders it a better proton shuttle or
20 directing agent, as it both attracts and releases.^{12, 17} Nevertheless, its incorporation into synthetic
21 molecular catalysts for proton reduction has been thusfar limited.^{15, 18-19}

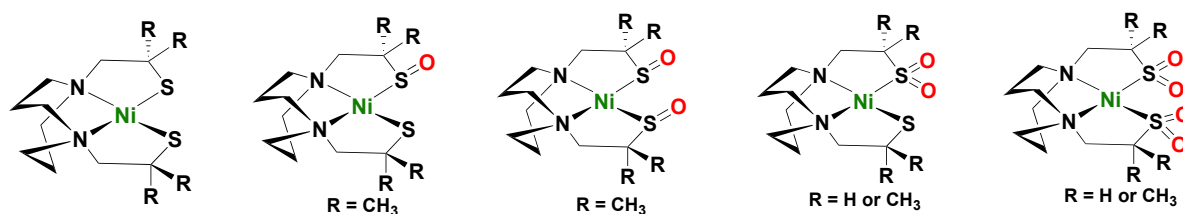
22
23
24 Upon exposure of a [NiFeS]-H₂ase to O₂, the active site deactivates to the so-called “Ni-
25 A” (unready) and “Ni-B” (ready) states.⁸ The more O₂-tolerant [NiFeS]-H₂ases are known to form
26 “Ni-B” displayed as a bridging hydroxo ligand between Ni(III) and Fe(II), **Figure 1**.²⁰ When
27 electron and protons from the normal reductive processes are pumped into this ready state, the
28 oxygen is quickly removed (t < 1 min) as H₂O and catalytic activity is recovered.^{2,21-24} However,
29 the “Ni-A” state, with a possible hydroxo bridge between Ni(III) and Fe (II) as well as a bridging
30 sulfenate, requires longer times (t > 1 h) to be reactivated.^{25, 2} Several structures of these
31 oxygenates have been determined by crystallography, and signals of their presence have long been
32 known from EPR studies which identified Ni(III) as the redox level in these off-cycle species.²⁶⁻
33
34
35
36
37
38
39
40
41
42
43
44
45
46
47
48
49
50
51
52
53
54
55
56
57
58
59
60
27, 1Studies by Lenz and Zebger, et al., show that the conversion of Ni-A to Ni-B in soluble NAD⁺-
reducing [NiFe] hydrogenase could proceed via oxygenation of the bridging sulfur in Ni-B, whose
active site is a structure similar to another unready state found by Fontecilla-Camps.²⁸⁻²⁹ It should
be pointed out that some 15 to 20 structures with varying degrees of oxygenation at metal or
chalcogen in [NiFeS] and [NiFeSe]-H₂ases active sites are found in the protein data bank (PDB)
as of this publication. We selected a subset of these to describe in Figure 1. Undoubtedly there will
be more in the future.

In contrast to the [NiFeS]-H₂ase, oxygen-damage of [NiFeSe]-H₂ase results in various O-
uptake levels, none of which feature paramagnetic Ni(III); however selenium and/or sulfur are
found oxygenated or oxidized as dichalcogenides in the structures.³⁰⁻³¹ Such oxygenation products
of [NiFeSe]-H₂ase, as well as of [NiFeS]-H₂ase active sites, can be interpreted as prevention or
protection, avoiding further metal oxidation and degradation of the Ni-Fe core structures in
each.^{19a,b,30,31} Reductive repair processes return the enzymes' function in both cases.³²

Recent reports from Pereira, et al., have provided key experiments that constrain the differences in activity of [NiFeSe]- and [NiFeS]-H₂ases to selenium itself rather than any structure changes in the protein.³³ Thus the simplest explanations for the greater hydrogenase activity and easier reactivation of oxygen-degraded [NiFeSe]-H₂ase as contrasted to the all-sulfur analogue lie in the greater polarizability of selenium, and the weaker Se-O bonds as contrasted to S-O.¹⁷ As such soft descriptions are difficult to quantify we have pursued relevant structure/function analyses in well-characterized heterobimetallic synthetic analogues containing S and Se. Our ultimate goal is to interpret the clues from synthetic models and from nature that might guide development of robust, oxygen-tolerant and cheap molecular catalysts for the hydrogen evolution/oxidation reaction.

Examples of S-oxygenated thiolates are plentiful in monomeric complexes containing nickel bound within a rigid tetradentate N₂S₂ ligand field; several examples are displayed in **Figure 1**.³⁴⁻³⁸ In fact, the single oxy-sulfur species, or sulfenate, was used to assemble the first reported biomimetic of S-oxygenated [NiFe]-H₂ase, using FeBr₂ as the iron receiver.³⁹ The synthesis of nickel-iron bimetallic complexes containing both sulfur and selenium, thus providing faithful synthetic analogues of the active sites of [NiFeS]- and [NiFeSe]-H₂ases, represents a considerable challenge.^{19, 40-41} A strategy found to be successful in the preparation of synthetic analogues of the nickel superoxide dismutase, and for address of other questions in the bioinorganic chemistry of nickel, is the splitting of dimeric [NiN₂S]₂²⁺ by exogenous thiolates.^{30, 42-43} Adaptations of this strategy are responsible for the results presented below.

Examples of nickel sulf-oxygenates within rigid N₂S₂ ligand fields:³⁴⁻³⁸



Selected [NiFeS]- and [NiFeSe]-Hydrogenase oxygenated active sites:^{8, 20, 26-27}

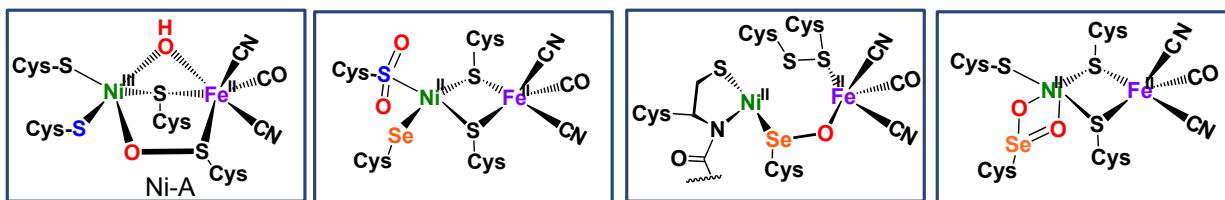


Figure 1. Selected S-oxygenated thiolates in monomeric nickel complexes, and examples from crystallography of oxygen-damaged [NiFe]-H₂ase active sites.^{8, 20, 26-27, 34-38} Note: these examples of the latter are taken from some 15 to 20 reported structures.

Results and Discussion

Minimal models of [NiFe]-H₂ase active site core structure are accessed from the cleavage of dimeric [NiN₂S]₂²⁺ complexes by various nucleophiles,⁴³ including aryl chalcogenides, E_{PHH}⁻, E

= S and Se.⁴¹ Unlike the stable S-oxygenates described in **Figure 1**, the resulting monomeric $\text{Ni}(\text{E}_{\text{PhX}})(\text{S}'_{\text{N}_2})$ complexes are air-sensitive resulting in degradation. Nevertheless, when combined with $(\eta^5\text{-C}_5\text{H}_5)\text{Fe}^{\text{II}}(\text{CO})(\text{CH}_3\text{CN})_2^+$, displacing the CH_3CN labile ligands, the resultant Ni-Fe complexes provide examples of stable products of O_2 uptake, **Figure 2**. While these models are imperfect structural analogues, our NiFe small molecules offer a paradigm for contrasting S and Se in relevant O_2 -addition and repair processes representative. Moreover, the arylchalcogenides are susceptible to modifications by para-substituents on the arene,⁴⁴ giving clues regarding electronic effects operative on oxygen uptake and product distribution. A summary of the reactions explored in this study is found in **Figure 2**.

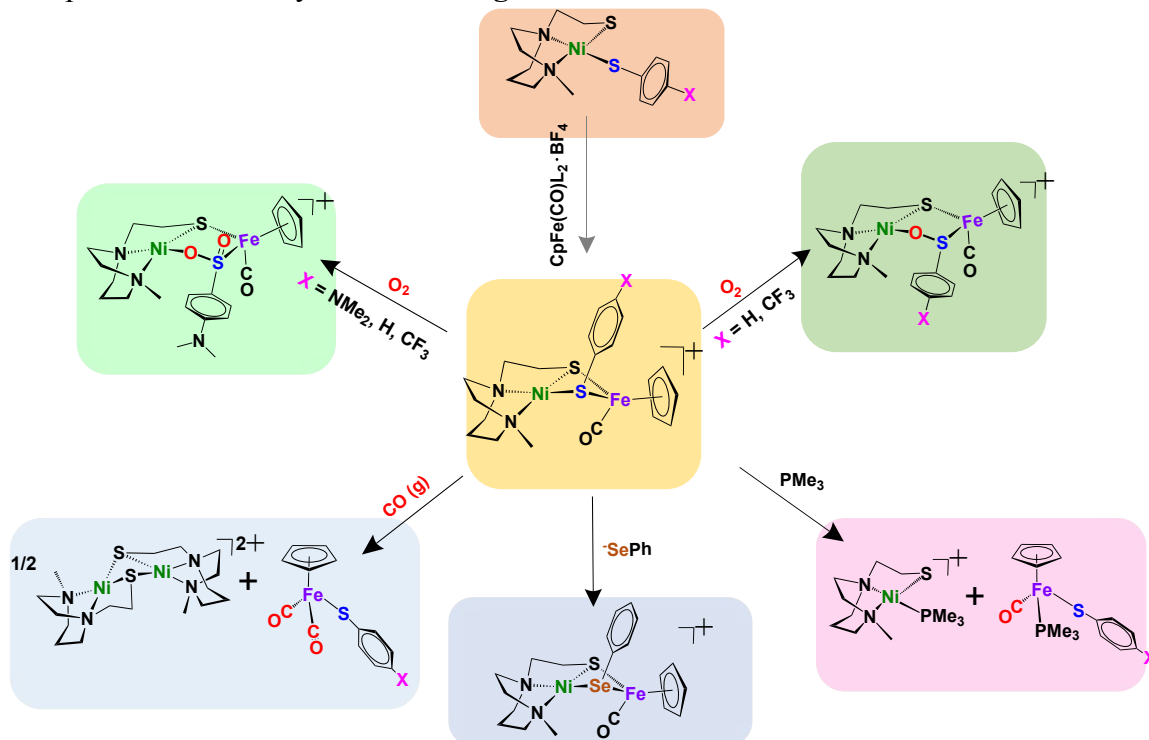


Figure 2. Synthesis of NiFe complexes containing para-substituted arylthiolates and various reactions. L in the $\text{CpFe}(\text{CO})\text{L}_2^+$ synthon, 12 o'clock arrow position, is CH_3CN as labile ligand. In all products the Ni and Fe are in +2 oxidation states.

Synthesis and Characterizations. The synthetic methods and characterizations (mass spectra, elemental analyses, ^1H NMR spectra, UV and CV spectra, and XRD crystal structures) are further detailed in the supplementary information. Monomeric $\text{Ni}(\text{S}_{\text{PhH}})(\text{S}'_{\text{N}_2})$,⁴¹ and *para*-substituted aryl derivatives, $\text{Ni}(\text{S}_{\text{PhX}})(\text{S}'_{\text{N}_2})$, ($\text{X} = \text{CF}_3, \text{Cl}, \text{H}, \text{OMe}, \text{NMe}_2$) complexes, were derived from the $[\text{NiN}_2\text{S}]_2^{2+}$ ([1-(2-mercaptoethyl)-methyl-1,4-diazacycloheptane] nickel(II)) dimer cleaved by the appropriate -S_{PhX} . The $\text{Ni}(\text{S}_{\text{PhX}})(\text{S}'_{\text{N}_2})$ complexes readily displaced acetonitrile in the $(\eta^5\text{-C}_5\text{H}_5)\text{Fe}^{\text{II}}(\text{CO})(\text{MeCN})_2^+$ precursor to generate diamagnetic, thermally stable $\text{Ni}(\mu\text{-S}_{\text{PhX}})(\mu\text{-S}'_{\text{N}_2})\text{Fe}$, ($\text{Fe} = (\eta^5\text{-C}_5\text{H}_5)\text{Fe}^{\text{II}}(\text{CO})^+$; $\text{X} = \text{CF}_3, \text{Cl}, \text{H}, \text{OMe}, \text{NMe}_2$) as rudimentary synthetic analogues of the $[\text{NiFeS}]\text{-H}_2\text{ase}$ active sites. **Figure 2** summarizes the synthetic scope as well as

reactivities explored in this study. The reaction profiles, including O₂ uptake, will be described in separate sections below. A selection of analogous Ni(μ-Se_{PhX})(μ-S'_{N2})Fe, (X = CF₃, H, NMe₂) complexes were similarly prepared and isolated. See the S.I. for details.

Molecular structures. Dark purple, X-ray quality, block crystals of the monomeric Ni(S_{PhX})(S'_{N2}) complexes were obtained by diethyl ether vapor diffusion into a solution of CH₃CN. The heterobimetallic, cationic Ni(μ-S_{PhX})(μ-S'_{N2})Fe complexes were isolated as BF₄⁻ salts and crystallized as dark brown blocks from a pentane-layered CH₂Cl₂ solution at -35 °C. The X substituents on the aryl ring do not substantially modify the structures. The monomeric Ni complexes crystallize in the P2₁/c (X = CF₃), P-1 (X = Cl) and Pbcn (X = NMe₂) space groups and feature minimally distorted NiN₂S₂ square planes. The full structural reports of the complexes in **Figure 3** are deposited in the Cambridge Data Base, and selected metric data are tabulated in the Supporting Information (Figure S43).

The Ni(μ-S_{PhX})(μ-S'_{N2})Fe complex structures feature square planar Ni(S_{PhX})(S'_{N2}) units connected by chalcogenide bridges into the typical piano-stool geometry about the [(η⁵-C₅H₅)Fe(CO)]⁺ unit, resulting in butterfly-like Ni-S-Fe-S' cores. The hinge angles, defined as the intersection of the best N₂SS' plane with the SS'Fe plane, are in the range of 135-141°. The Ni^{II} - - Fe^{II} distances of 3.1 – 3.2 Å, are beyond the possibility of a metal-metal bond. Earlier we reported the XRD structures of the Ni(μ-Se_{PhH})(μ-S'_{N2})Fe with the Ni^{II} - - Fe^{II} distance = 3.253 Å, and the mono-oxy derivative of the phenyl-selenolate. The expanded 5-membered metallocycle seen in the latter, the 2 o'clock position of **Figure 2**, has a slightly larger Ni^{II} - - Fe^{II} distance, 3.568 Å. In the current study, only the X = NMe₂ derivative provided x-ray quality crystals from reaction of Ni(μ-S_{PhX})(μ-S'_{N2})Fe with O₂. The structure displays a sulfinate unit in the 5-membered Ni-O-S(=O)Fe-S' ring, with Ni^{II} - - Fe^{II} distance = 3.395 Å. In summary, neither the 2-oxy or the mono-oxy products show significant modification of the Ni-Fe bimetallic structures.

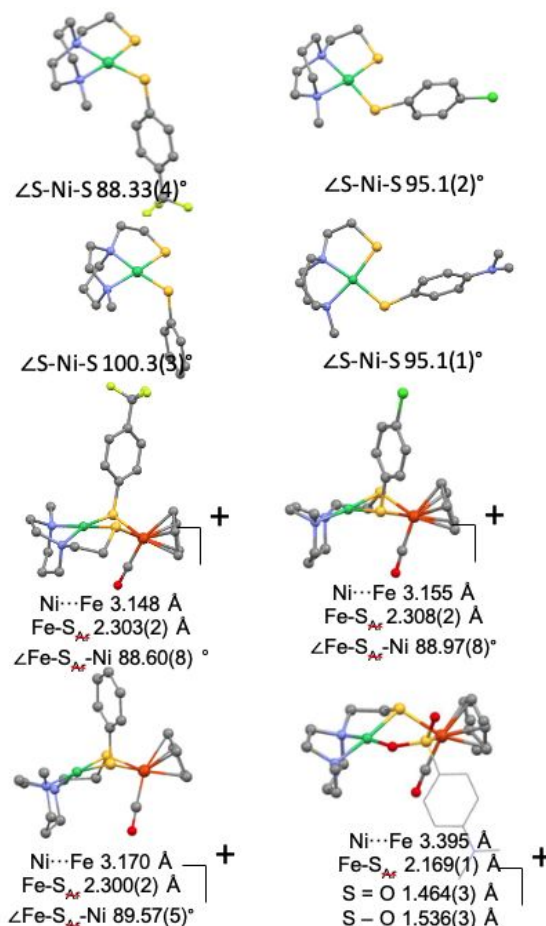


Figure 3. Molecular XRD structures determined for monomeric Ni and for the Ni(μ-S_{PhX})(μ-S'_{N2})Fe complexes. Full listings of metric data are in the Supplementary Information.

IR spectra and electrochemical characterizations. Correlations of the Hammett σ_p parameter with $\nu(\text{CO})$ IR values and $\text{Ni}^{\text{II/I}}$ reduction potentials derived from cyclic voltammetry, for the series of NiFe complexes are presented as plots in **Figure 4**.⁴⁴ Both theoretical (DFT-derived values) and experimental data of the $\nu(\text{CO})$ in $\text{Ni}(\mu\text{-S}_{\text{PhX}})(\mu\text{-S}'_{\text{N}_2})\text{Fe}$ and E_{cathode} potentials for $\text{Ni}^{\text{II/Ni}^{\text{I}}}$ in monomeric $\text{Ni}(\text{S}_{\text{PhX}})(\mu\text{-S}'_{\text{N}_2})$ complexes conform with the Hammett parameters of the X substituents on the -S_{PhX} ligands. Specifically, more electron-donating substituents result in lower $\nu(\text{CO})$ values, illustrating electronic communication over 5 bonds and the influence on π -backbonding from Fe^{II} to the CO. The $\text{Ni}(\mu\text{-Se}_{\text{PhX}})(\mu\text{-S}'_{\text{N}_2})\text{Fe}$ series shows $\nu(\text{CO})$ responses to X similar to the sulfur analogues, however moderated in value. Interestingly, the phenyl derivative with the most electron-donating substituent, $\text{Ni}(\mu\text{-S}_{\text{PhNMe}_2})(\mu\text{-S}'_{\text{N}_2})\text{Fe}$, gives same $\nu(\text{CO})$ value (1934 cm^{-1}) as found in $\text{Ni}(\mu\text{-Se}_{\text{PhH}})(\mu\text{-S}'_{\text{N}_2})\text{Fe}$. There is not such a match in the $\text{Ni}^{\text{II/I}}$ reduction potential.

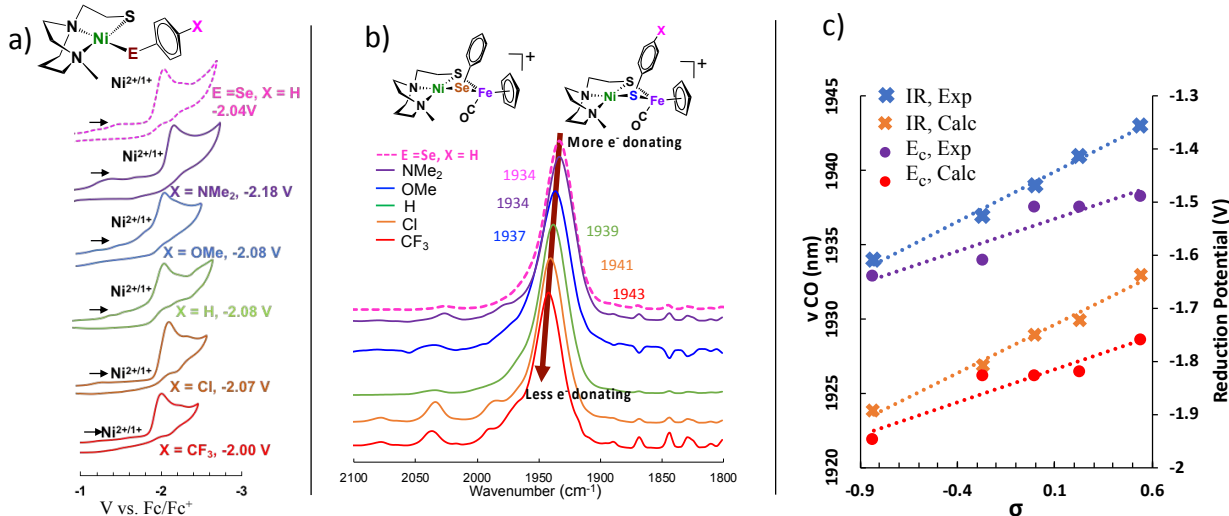


Figure 4. a) Cyclic voltammograms in E_c region for $\text{Ni}^{\text{II/Ni}^{\text{I}}}$ and monomeric Ni complexes; b) The $\nu(\text{CO})$ IR spectra of $\text{Ni}(\mu\text{-E}_{\text{PhX}})(\mu\text{-S}'_{\text{N}_2})\text{Fe}$; c) Correlations of Hammett σ parameters with experimental and calculated $\nu(\text{CO})$ values and E_c values of $\text{Ni}^{\text{II/Ni}^{\text{I}}}$ in $\text{Ni}(\mu\text{-S}_{\text{PhX}})(\mu\text{-S}'_{\text{N}_2})\text{Fe}$.

Computational Section I. DFT calculations were performed using the TPSSSTPSS functional with the 6-311++G(d,p) basis set on the nonmetal atoms and the 6-311+G basis set on nickel and iron in the Gaussian 16 suite.⁴⁵ The molecular structures from XRD presented above were used as geometric starting points with all other structures made by the appropriate atomic substitutions in the AMPAC Graphical User Interface (AGUI)⁴⁶. All structures were optimized in solvent by using the SMD solvation model with acetonitrile as the solvent. Vibrational frequencies were calculated ‘in solvent’ and all species were confirmed to be minimum energy structures by the absence of an imaginary frequencies. Standard statistical mechanical and solvation corrections were applied to the electronic energy of the optimized structures to give free energy values (standard states were not converted to mol/L).

1
2
3 The computational methods yielded the structures and energies of the $\text{Ni}(\mu\text{-S}_{\text{PhX}})(\mu\text{-S}'_{\text{N}_2})\text{Fe}$ complexes as well as their singly and doubly oxygenated forms. These calculations aimed
4 to examine how the properties of the model complexes depended on the chalcogen identity, sulfur
5 vs. selenium, and with para substituents, X, that modified the electron-donating properties of the
6 E-PhX. Our computational method accurately reproduces the trends seen in the experimental data
7 for structures (where available), the trends in $\nu(\text{CO})$ IR values (absolute values are underestimated),
8 and the positions of $\text{Ni}^{\text{II/I}}$ reduction potentials (**Figure 4**).
9

10
11 Mentioned above, the $\text{Ni}(\mu\text{-E}_{\text{PhX}})(\mu\text{-S}'_{\text{N}_2})\text{Fe}$ complexes with E = Se, X = H and with E =
12 S, X = NMe_2 display the same $\nu(\text{CO})$ values in experiment (1934 cm^{-1}) and from theory (1895
13 cm^{-1}). These equivalent values indicate that, as relayed by iron to the carbon monoxide ligand, the
14 Se_{PhH} and the $\text{S}_{\text{PhNMe}_2}$ are equally strong electron donors. Similarly, the calculated $\nu(\text{CO})$ stretch
15 for the singly oxygenated $\text{Ni}(\mu\text{-O-}\mu\text{-Se}_{\text{Ph}})(\mu\text{-S}'_{\text{N}_2})\text{Fe}$ (1919 cm^{-1}) is comparable to that of $\text{Ni}(\mu\text{-O-}$
16 $\text{S}_{\text{PhNMe}_2})(\mu\text{-S}'_{\text{N}_2})\text{Fe}$ (1921 cm^{-1}). In contrast with the doubly oxygenated complexes the $\nu(\text{CO})$
17 value calculated for the two-oxy species, the $\text{Ni}(\mu\text{-O-(O=)Se}_{\text{PhH}})(\mu\text{-S}'_{\text{N}_2})\text{Fe}$ complex (1936 cm^{-1})
18 is now most similar to the sulfur analogue with the electron withdrawing X = CF_3 , i.e., $\text{Ni}(\mu\text{-O-}$
19 $\text{S(=O)}_{\text{PhCF}_3})(\mu\text{-S}'_{\text{N}_2})\text{Fe}$. There are minor differences in for the three di-oxy selenium species.
20 **Table S1** lists $\nu(\text{CO})$ values of all species that were derived experimentally and also the DFT
21 calculated values.
22
23
24
25
26
27
28

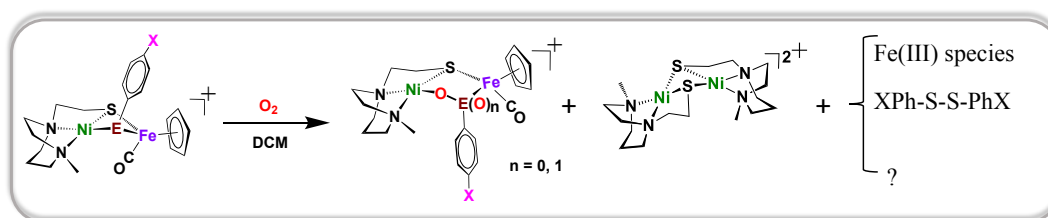
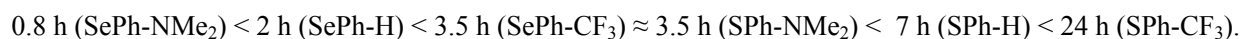
29 **Chemical Reactivity.** Various chemical reactions of $\text{Ni}(\mu\text{-S}_{\text{PhX}})(\mu\text{-S}'_{\text{N}_2})\text{Fe}$ complexes are
30 presented in **Figure 2**. In the $\text{Ni}(\mu\text{-S}_{\text{PhX}})(\mu\text{-S}'_{\text{N}_2})\text{Fe}$ series, the Se_{PhH} ligand is found to replace the
31 S_{PhX} to form $\text{Ni}(\mu\text{-Se}_{\text{PhH}})(\mu\text{-S}'_{\text{N}_2})\text{Fe}$ in low yield along with degradation products. Under $\text{CO}(\text{g})$,
32 the $\text{Ni}(\mu\text{-S}_{\text{PhX}})(\mu\text{-S}'_{\text{N}_2})$ complexes cleanly convert into dimeric $[\text{NiN}_2\text{S}]_2^{2+}$ and $(\eta^5\text{-C}_5\text{H}_5)\text{Fe}(\text{CO})_2\text{S}_{\text{PhX}}$.
33 With PMe_3 , the $\text{Ni}(\mu\text{-S}_{\text{PhX}})(\mu\text{-S}'_{\text{N}_2})\text{Fe}$ also easily cleaves into two products:
34 $\text{Ni}(\text{S}'_{\text{N}_2})(\text{PMe}_3)$ and $(\eta^5\text{-C}_5\text{H}_5)\text{Fe}(\text{CO})(\text{PMe}_3)\text{S}_{\text{PhX}}$. In summary, a) the reactivity of $\text{Ni}(\mu\text{-S}_{\text{PhX}})(\mu\text{-S}'_{\text{N}_2})\text{Fe}$
35 with the poor nucleophile, CO, is controlled by S_{PhX} , shifting to Fe with concomitant
36 release of $[\text{Ni}(\text{S}'_{\text{N}_2})]^+$, readily scavenged by another of itself forming the thermodynamically stable
37 $[\text{NiN}_2\text{S}]_2^{2+}$; b) with the good nucleophile, PMe_3 , both the Ni and Fe products contain PMe_3 . The
38 fact that S_{PhX} prefers the Fe^{II} rather than Ni^{II} is consistent with the observation of oxygen insertion
39 between Ni and S_{Ph} that leaves the sulfur of S_{PhX} bound to Fe, *vide infra*.
40
41
42
43
44

45 **Reactions with O_2 .** Three $\text{Ni}(\mu\text{-S}_{\text{PhX}})(\mu\text{-S}'_{\text{N}_2})\text{Fe}$ and three $\text{Ni}(\mu\text{-Se}_{\text{PhX}})(\mu\text{-S}'_{\text{N}_2})\text{Fe}$ complexes were
46 selected for studies of O_2 reactivity: X = NMe_2 (most electron-donating); X = H; and X = CF_3
47 (most electron-withdrawing). Details of the experimental protocol are deposited in the Supporting
48 Information (p.S4, Synthesis and Characterization Section). Dichloromethane solutions of the
49 NiFe complexes were sparged with O_2 for 30 min at $22\text{ }^\circ\text{C}$. The reactions were monitored by $\nu(\text{CO})$
50 FTIR spectroscopy until no further changes, followed by celite filtration and isolation of the S-
51 oxygenated products by solvent removal. Mass spectroscopy (^+ESI) was used to identify the
52 components in the product mixture. A summary of results is found in **Figure 5**. In all cases, the
53 byproducts were the disulfide, XPhS-SPhX , and the dimeric species, $[\text{NiN}_2\text{S}]_2^{2+}$. The presence of
54
55
56
57
58
59
60

an Fe^{III} species isolated from residual solids was established by addition of aqueous Na⁺SCN⁻ with formation of the blood red [Fe(SCN)(H₂O)₅]²⁺ complex.

Under identical conditions for Ni(μ-S_{PhX})(μ-S'_{N₂})Fe derivatives of three arene substituents, we compared the O₂ reaction times and yields of the principal products. In the case of X = H, 7 h are required to complete the O₂ reaction, yielding a mixture of the mono- and di-oxy species with overall yield of 37%.⁴¹ In contrast, when X = CF₃, the reaction required 24 h to maximize the products from the reduced form, with ν(CO) at 1943 cm⁻¹, to oxygenated products (a mixture of 1-oxy and 2-oxy species) that displayed as an unresolved broad ν(CO) band at 1971 cm⁻¹. The isolated yield was *ca.* 30%. With the Me₂N substituent, the major product is the di-oxy species, isolated in 55% yield after 3.5 h.

For comparison, the Ni(μ-Se_{PhH})(μ-S'_{N₂})Fe completed reaction with O₂ after only 2 h, giving a 56% yield of sulf-oxygenated products predominantly of the mono-oxy type.⁴¹ Modifications using CF₃ and NMe₂ as para-substituents in -Se_{PhX} gave slower (3.5 h) and faster (0.8 h) reactions with O₂, respectively. In summary, while selenium analogues are more reactive than sulfur, both the selenolate and thiolate bridges respond to the X substituent on the aryl groups. The more electron-donating substituent in the aryl-substituted chalcogenide ligands, Ni(μ-E_{PhX})(μ-S'_{N₂})Fe, gave greater yields and more rapid E-oxygenation reactions. The reaction time profile is as follows:



E-X	σ	Reaction time	Main Product	Combined Yield of Oxygenate(s)
S-NMe ₂	-0.830	3.5 h	2-Oxy Species	55 %
S-H	0.000	7 h	Mixture (n = 0, 1)	37 %
S-CF ₃	+0.540	24 h	Mixture (n = 0, 1)	30 %
Se-NMe ₂	-0.830	0.8 h	1-Oxy Species	61 %
Se-H	0.000	2 h	1-Oxy Species	56 %
Se-CF ₃	+0.540	3.5 h	Mixture (n = 0, 1)	40 %

Figure 5. The reactions of Ni(μ-E_{PhX})(μ-S'_{N₂})Fe complexes dissolved in CH₂Cl₂ under 1 atm O₂ at room temperature. Reaction time is defined as that required to reach a plateau of the product ν(CO) band. Attempts to separate or determine the distribution in the mixtures of 1- and 2-oxy products were unsuccessful. Components of product mixtures identified by ⁺ESI-Mass spectrometry.

1
2
3
4
5 The identical $\nu(\text{CO})$ absorptions (1934 cm^{-1}) of the $\text{Ni}(\mu\text{-Se}_{\text{PhH}})(\mu\text{-S}'_{\text{N}_2})\text{Fe}$ and the $\text{Ni}(\mu\text{-S}_{\text{PhNMe}_2})(\mu\text{-S}'_{\text{N}_2})\text{Fe}$ complexes are reasonably connected to their oxygen reactivity which is significantly greater than the congeners in the series. While the electron density reported by π -back-bonding of iron to CO appears to be the same in the two complexes, a difference exists in reactivity (time to completion) and product distribution. A single O-uptake for $\text{Ni}(\mu\text{-Se}_{\text{PhH}})(\mu\text{-S}'_{\text{N}_2})\text{Fe}$ leads to the selenoate, Ni-O-Se-Fe-S' bridge between Ni and Fe; a 2-oxy addition, with production of a bridging sulfinato complex, Ni-O-S(=O)-Fe, is seen for product (>90% of the 2-oxy species) from $\text{Ni}(\mu\text{-S}_{\text{PhNMe}_2})(\mu\text{-S}'_{\text{N}_2})\text{Fe}$.

16
17 **Computational Section II.** The O-uptake distinctions in the Ni—Fe complexes inspired further DFT computations that addressed thermodynamic driving forces for O_2 reactions and the two types of products. Summarized in **Figure 6** are free energies, ΔG° , for the sulfur and selenium single oxygenation reactions found to be similar at -14.3 and -15.6 kcal/mol, respectively. The double oxygenation reactions however show a greater difference; the ΔG° in the selenium case is -25.2 kcal/mol whereas the sulfur case is favored by -35.5 kcal/mol. The selenium 2-oxy species is more stable than the 1-oxy but the energy gap between the levels (9.6 kcal/mol) is approximately half as large as the energy gap for the sulfur analogues (21.1 kcal/mol). While the reaction energies indicate in both cases the 2-oxy species should be the thermodynamic product, only the sulfur displays the sulfinato. In the absence of a mechanism for the O_2 uptake reaction we suggest possible working hypotheses: #1) the selenium 2-oxy product is less kinetically accessible than the 1-oxy product; or #2) the 2-oxy product is formed but the weak terminal Se=O, see below, allows the complex to undergo comproportionation with the mixed chalcogenide precursor to form two equivalents of 1-oxy products. This type of reactivity has no direct analog in enzymes due to the enclosed nature of the active site.

36 Reasonable support for hypothesis #2 is that the difference in the ΔG° for the 2-oxy complexes correlates with the strength of the π bond to the terminal oxygen for sulfur vs. selenium. The Natural Bond Orbital (NBO)⁴⁷ analysis (second order perturbation) reveals the total stabilization energy coming from interactions of the lone pairs on the terminal oxygen with the chalcogen to be 24.4 kcal/mol for the sulfur and 13.0 kcal/mol for the selenium variant. While the natural atomic orbitals that make up the S=O and Se=O π interaction (details in the SI) appear nearly identical, the greater electronegativity difference for Se and the greater orbital size mismatch for Se results in the weaker π bond with the terminal oxygen as compared to sulfur.

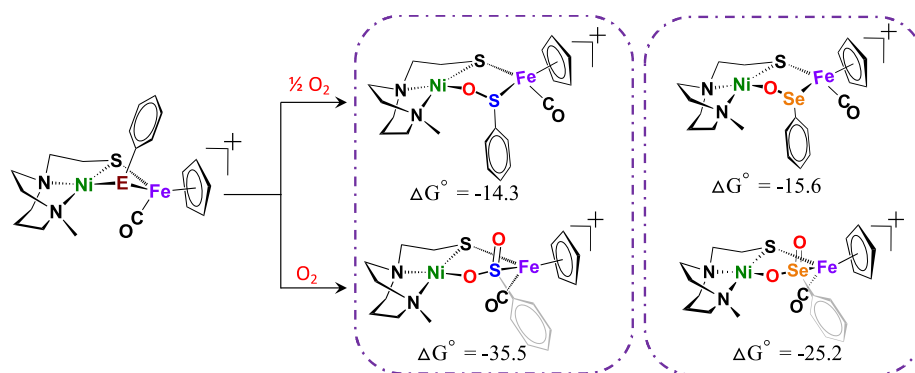


Figure 6: DFT calculated free energy values, ΔG° , for comparison of oxygen-uptake reactions of $\text{Ni}(\mu\text{-E}_{\text{PhH}})(\mu\text{-S}'\text{N}_2)\text{Fe}$ complexes, E = S and Se, in kcal/mol.

Mechanism of O_2 addition—*isotopic labeling.*

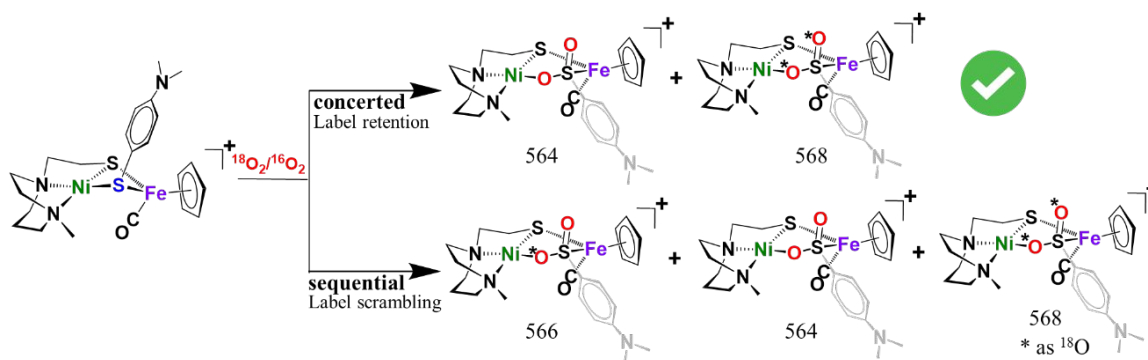


Figure 7. Predicted concerted and sequential mechanisms for the reactions of $\text{Ni}(\mu\text{-S}_{\text{PhX}})(\mu\text{-S}'\text{N}_2)\text{Fe}$ complexes with $^{18}\text{O}_2$.

Notably, the addition of O₂ in the case of X = NMe₂ in **Ni**(μ-S_{PhX})(μ-S'_{N2})**Fe**, cleanly yields the 2-oxy-sulfur, or sulfinato, complex as the main oxygenate. We addressed the question of concerted addition of the oxygen atoms from one O₂ molecule or stepwise addition from separate O₂ molecules by isotopic labeling/crossover experiments, as shown in **Figure 7**. A mixture of ¹⁸O₂/¹⁶O₂ (in ratio of 38:62) gas was added to a CH₂Cl₂ solution of **Ni**(μ-S_{PhNMe2})(μ-S'_{N2})**Fe** complex, and isolated products were subjected to mass spectrometric analysis in order to determine the isotope distribution in the product sulfinato complex. If a concerted mechanism prevails, the di-oxy product should retain the labels of the O₂ substrate; if stepwise addition, there should be evidence of label scrambling, the ¹⁶O¹⁸O sulfinato product. Isotopic bundle analysis finds an isotopomer at the mass peak of 566 m/z which is distinctive as an indicator for label scrambling. The theoretical distributions in the ion bundle are shown in **Figure 8** along with the experimental result for the specific mixture of ¹⁸O₂/¹⁶O₂.

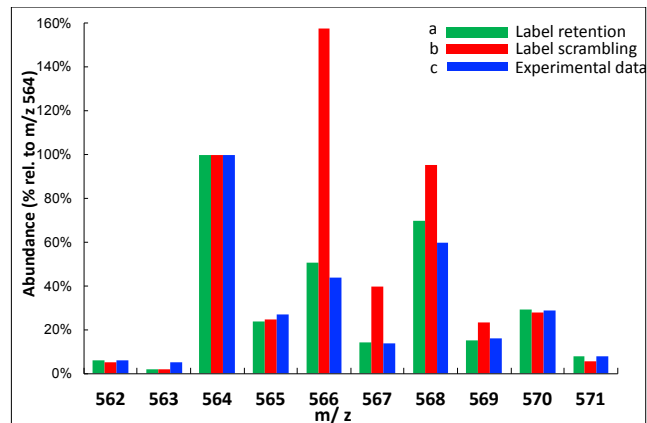


Figure 8. Theoretical and experimental ion abundances for the mass spectrum in the [M + 2O]⁺ region from the reaction of **Ni**(μ-S_{PhNMe2})(μ-S'_{N2})**Fe** with a 62:38 mixture of ¹⁶O₂:¹⁸O₂ (a) by label retention; (b) by label scrambling; and (c) the experimental results.

From the lack of a match of the m/z 566 signal we conclude that the experimental reaction mixture best fits label retention; i.e., the isotopomeric di-oxy products are Ni¹⁶O¹⁶O SFe and Ni¹⁸O¹⁸O SFe, and the two oxygens on sulfur are from one oxygen molecule. This agrees with previous studies on monomeric NiN₂S₂ complexes featuring terminal *cis*-dithiolates, **Figure 1**, that have shown that the addition of ³Σ O₂ proceeds primarily through a concerted mechanism to produce both bisulfenates (RSO⁻) as well as mono- and bisulfates (RSO₂).^{35, 38}

Oxygenated chalcogenide repair. Earlier we determined that the O atom in the mono-oxy, μ-O, μ-E_{Ph}, complexes could be rapidly removed by PR₃ (R = Me or o-tolyl) in both the sulfur and selenium cases, regaining the μ-E_{Ph}.⁴¹ However, electrochemical reductions in the presence of acid were ineffective towards removal of the O-atom as H₂O. In the current study, Cp₂Co was adopted as an electron source and HBF₄ as proton source. A dark reddish-brown CH₂Cl₂ solution of Ni-O-Se_{PhH}-Fe, with ν(CO) 1954 cm⁻¹, was cooled to -78 °C and transferred into a pre-cooled flask containing 2 equiv of Cp₂Co powder whereupon a reduced, dark green, CO-containing species of unknown composition was formed, **Figure 9**. On subsequent addition of 2 equiv of HBF₄ a gradual color change back to dark brown was observed over 1.5 h, along with a shift in the ν(CO) to 1934 cm⁻¹, indicating with O-atom removal and a spectroscopic yield of 60%. The ⁺ESI-Mass spectrum confirmed the deoxygenation and return to **Ni**(μ-Se_{PhH})(μ-S'_{N2})**Fe**. Infrared and proton NMR spectroscopies indicated that the oxygen was removed as H₂O. An experiment with the 1-oxy-sulfur analogue, Ni-O-S_{PhH}-Fe as a mixture with the 2-oxy species, indicated reduction of the

former, however the sulfinato species was not affected. Addition of excess Cp_2Co resulted in overall degradation/decomposition.

To further examine the O-removal from the sulfinato, we took the isolated two-oxy species or sulfinato complex, Ni-O-S(=O)Fe in the case of X = NMe₂ and attempted the “repair” using Cp_2Co and HBF_4 . After adding Cp_2Co , the intensity of $\nu(\text{CO})$ 1960 cm^{-1} decreased but no new band was observed even after 6 h, or with increased amounts of HBF_4 . Further analysis of ⁺ESI-Mass spectrum indicates a low intensity signal at m/z 564 for the 2-oxy species but no indication of the reduced species, either 1-oxy or the NiSFe parent complex.

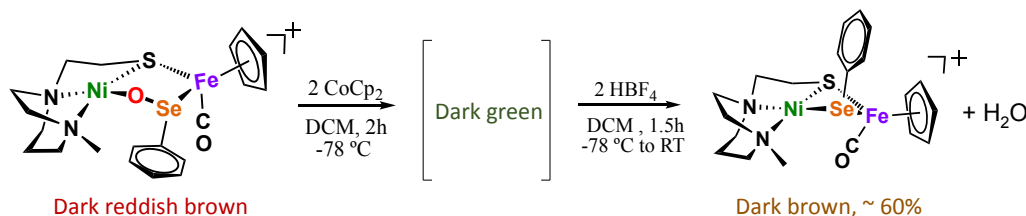


Figure 9. Oxygen removal reaction using Cp_2Co as reductant and HBF_4 .

The model repair process shown in Figure 9 is of relevance to the soluble, NAD^+ -reducing [NiFe]-H₂ase from *R. eutropha*, whose S-oxygenated active site has been suggested to be reversible under O_2 and NADH/H^+ .^{28,52} In the proposed mechanism for the latter, the S-mono-oxygenate is reduced by NADH ; with added H^+ producing H_2O . Similarly, in our repair process, the reductant Cp_2Co analogous to NADH , and along with the H^+ , removes the O atom as H_2O .

Conclusions and Final Remarks

The salient features of this study follow:

- The nominal models of [NiFeS]- and [NiFeSe]-H₂ase active sites described above with bridging chalcogenides function as a probe of O_2 reactivity that yield isolable NiFe complexes where thiolate and selenolate are converted into sulf- and seleno-oxygenates. The presence of a carbon monoxide reporter ligand on Fe offered opportunity to explore “electronic alchemy” through remote effects of substituents on the E_{PhX} ligand that effectively (electronically) transformed S into Se. Preliminary Mossbauer studies find simple quadrupole doublets and nearly identical isomer shifts for the parent Ni-Fe-S and Ni-Fe-Se reduced complexes. Thus, the increased electron density from the Se that influences the $\nu(\text{CO})$ IR values via Fe^{II} has no effect on the iron nuclei.
- The stability of these NiFe complexes, even under siege by O_2 , is impressive. Crystallography finds only minimal changes in the coordination sphere of the bimetallic complex; the NiFe core is maintained with marginal differences in the Ni--Fe distances even though the E_{PhX} bridging ligand has been expanded into an Ni-O-S-Fe or Ni-O-Se-Fe unit.

1
2
3 c) Supported by earlier DFT computations,⁴¹ we surmise that the rigidity of the tridentate N₂S
4 “pincer” type ligand guides production of E-oxygenates at the more mobile, mono-dentate,
5 bridging E_{PhX} ligand site. Consistent with this conclusion are results from the Ogo group using
6 NiN₂S₂ (with N₂S₂ as a fixed tetradentate binding site for Ni^{II}) as metalloligand to Cp*Fe^{II}, bearing
7 an open site on iron.⁴⁸⁻⁵⁰ Under O₂ such Ni-Fe complexes yield isolable Fe^{IV}(peroxo) species, with
8 O₂²⁻ side-on bound to Fe in [NiN₂S₂-Fe(O₂)Cp*]⁺ rather than any of the S-oxygenates displayed
9 in **Figure 1**.
10
11
12

13
14 d) The oxidation states of Ni and Fe in the product oxygenates of our study remain at Ni^{II} and
15 Fe^{II} for both the selenium and the sulfur derivatives. However we note that low temperature (0 °C)
16 monitors of the O₂ reactions with the Ni-Fe containing the μ-S_{PhNMe₂} bridging ligand found a
17 buildup of a transient (but long-lived) EPR-active species as the reaction proceeded; a signal at
18 g_{avg} ≈ 2.09 is assigned to Ni^{III} while one at g = 4.19 is likely Fe^{III}, see Supporting Information
19 (Figure S60-62). At reaction’s end, oxygenated sulfurs were produced and the (presumed) Ni^{III}
20 signal had disappeared. Some byproduct containing iron(III) is found in the oxidized residue from
21 these reactions. These observations are reminiscent of the early EPR studies of [NiFe]-H₂ase redox
22 poised in different levels, which gave rise to signals for Ni-A and Ni-B.^{1, 26-27}
23
24
25
26

27 e) The preference of O-atom bridged S and Ni, that we observed here, is seen in the sulfenato
28 complex of O-damaged [NiFeS]-H₂ase, (**Figure 1**). The Ni-O-Se-Fe as a bridging unit is also
29 observed here, but it is opposite to the Ni-Se-O-Fe arrangement found in one of the forms of O-
30 damaged [NiFeSe]-H₂ase.³⁰⁻³¹ In fact, protein crystallography has uncovered a variety of
31 chalcogen-oxygenates and myriad binding modes in the structures of oxygen-damaged [NiFe]-
32 H₂ase enzyme active sites; such a display is likely a benefit of reaction within a restrictive enzyme
33 active site cavity that partially accounts for the longevity of these species. In contrast, in
34 oxygenated solutions containing our small molecule active-site analogues, serious oxygen
35 exposure and damage is likely to lead to intractable metal oxides.
36
37
38
39

40 f) While there are discernible variations in oxygen uptake and product distributions that show
41 correlations with electronic differences in the para-substituent series, the possible causes are many
42 and expected to be intricately interrelated. For example, enhancement of electron-rich character
43 at E in E_{PhX} from the para-substituent effect, increases the likelihood for O₂ binding both to E, S
44 or Se, as well as to the metals which they bridge. Assuming that the affinity for the E_{PhX} ligand
45 by Fe^{II} continues to be greater than to the Ni^{II}, then the O₂-uptake activity should be limited to the
46 two sites, Ni^{II} and ⁻E_{PhX}. Whether the O₂ activation by Ni precedes O-atom attachment to E is
47 unknown at this point; whether the mono-oxy species result from an initial di-oxy species in all
48 cases, is also unclear. A full computational mechanistic study will address such questions.
49
50
51
52

53 We have seen in these studies, consistent with the enzyme studies or results, that compared
54 to sulfur in nearly identical chemical environment, selenium exhibits more facility for O₂ uptake.¹⁷
55
56
57
58
59
60

1
2
3 The observed oxygenated Se product is a single oxy species (we cannot discount a di-oxy species
4 as intermediate), and O-atom removal is facile for selenium. Excellent commentaries regarding
5 “Why nature chose - -”^{17, 51} heavier elements in the chalcogen or pnictogen family for numerous
6 biological processes clearly point to their intricate interactions with oxygen. In hydrogenase
7 enzyme chemistry, the many benefits of selenium incorporation include not only enhancement of
8 catalytic activity through proton shuttling and hydrogen expulsion rates, but also of protection of
9 the active sites from the poisonous O₂. Such benefits apparently outweigh the added cost to the
10 organism of the biosynthesis. As of now, there are few synthetic HER or ORR molecular catalysts²
11 that target selenium substitution and explore possible paybacks for the minimal synthetic
12 expenditure. We hope that our results point to new directions in this regard.
13
14
15
16
17

18 **Associated Content**

19 ***Supplementary Information***

20 Experimental, characterizations, additional spectroscopic, preliminary Mössbauer and EPR studies,
21 and computational details (PDF)

22 X-ray Crystallographic data (CIF)

23 This material is available free of charge via the Internet at <http://pubs.acs.org>.
24
25
26

27 **Author Information**

28 Corresponding Authors:

29 *marcetta@chem.tamu.edu

30 *hall@science.tamu.edu
31
32
33

34 **Notes**

35 The authors declare no competing financial interest.
36
37

38 **Acknowledgement**

39 This work was financial supported by the National Science Foundation (CHE-1300787, CHE-
40 1664866 to M.B.H. and CHE-1665258 to M.Y.D.) and the Robert A. Welch Foundation (A-0648
41 to M.B.H. and A-0924 to M.Y.D.). We thank Kyle Burns, Waseem Vali, and Prof. Paul Lindahl
42 for the preliminary Mössbauer studies.
43
44
45

46 **References:**

- 47 1. Cammack, R.; Frey, M.; Robson, R. *Hydrogen as a Fuel*. Taylor and Francis: London and
48 New York, 2001.
- 49 2. Vincent, K. A.; Parkin, A.; Lenz, O.; Albracht, S. P. J.; Fontecilla-Camps, J. C.; Cammack, R.
50 F., B.; Armstrong, F. A. Electrochemical Definitions of O₂ Sensitivity and Oxidative Inactivation in
51 Hydrogenases. *J. Am. Chem. Soc.* **2005**, *127*, 18179-18189.
- 52 3. Wakerley, D. W.; Reisner, E. Oxygen-tolerant Proton Reduction Catalysis: Much O₂ about
53 Nothing? *Energy Environ. Sci.* **2015**, *8*, 2283-2295.
54
55
56
57
58
59
60

- 1
- 2
- 3
- 4 4. Buhrke, T.; Lenz, O.; Krauss, N.; Friedrich, B. Oxygen Tolerance of the H₂-sensing [NiFe]
5 Hydrogenase from *Ralstonia eutropha* H16 Is Based on Limited Access of Oxygen to the Active
6 Site. *J. Biol. Chem.* **2005**, *280*, 23791-23796.
- 7
- 8 5. Duche, O.; Elsen, S.; Cournac, L.; Colbeau, A. Enlarging the Gas Access Channel to the
9 Active Site Renders the Regulatory Hydrogenase HupUV of *Rhodobacter Capsulatus* O₂ Sensitive
10 Without Affecting Its Transducing Activity. *FEBS J* **2005**, *272*, 3899-3908.
- 11
- 12 6. Fritsch, J.; Lenz, O.; Friedrich, B. Structure, Function and Biosynthesis of O₂-tolerant
13 Hydrogenases. *Nat Rev Microbiol* **2013**, *11*, 106-114.
- 14
- 15 7. Lenz, O.; Ludwig, M.; Schubert, T.; Burstel, I.; Ganskow, S.; Goris, T.; Schwarze, A.;
16 Friedrich, B. H₂ Conversion in the Presence of O₂ as Performed by the Membrane-Bound [NiFe]-
17 Hydrogenase of *Ralstonia eutropha*. *Chemphyschem* **2010**, *11*, 1107-1119.
- 18
- 19 8. Lubitz, W.; Ogata, H.; Rudiger, O.; Reijerse, E. Hydrogenases. *Chem Rev* **2014**, *114*, 4081-
20 4148.
- 21
- 22 9. Pandelia, M.-E.; Fourmond, V.; Tron-Infossi, P.; Lojou, E.; Bertrand, P.; Le'ger, C.; Giudici-
23 Orticoni, M.-T.; Lubitz, W. Membrane-Bound Hydrogenase I from the Hyperthermophilic
24 Bacterium *Aquifex aeolicus*: Enzyme Activation, Redox Intermediates and Oxygen Tolerance.
25 *J. Am. Chem. Soc.* **2010**, *132*, 6991-7004.
- 26
- 27 10. Shomura, Y.; Yoon, K. S.; Nishihara, H.; Higuchi, Y. Structural Basis for a [4Fe-3S] Cluster
28 in the Oxygen-tolerant Membrane-bound [NiFe]-hydrogenase. *Nature* **2011**, *479*, 253-256.
- 29
- 30 11. Volbeda, A.; Amara, P.; Darnault, C.; Mouesca, J. M.; Parkin, A.; Roessler, M. M.;
31 Armstrong, F. A.; Fontecilla-Camps, J. C. X-ray Crystallographic and Computational Studies of the
32 O₂-tolerant [NiFe]-hydrogenase 1 from *Escherichia coli*. *Proc. Natl. Acad. Sci. U. S. A* **2012**, *109*,
33 5305-5310.
- 34
- 35 12. Baltazar, C. S. A.; Marques, M. C.; Soares, C. M.; DeLacey, A. M.; Pereira, I. A. C.; Matias,
36 P. M. Nickel-Iron-Selenium Hydrogenases - An Overview. *Eur. J. Inorg. Chem.* **2011**, *2011*, 948-
37 962.
- 38
- 39 13. De Lacey, A. L.; Gutierrez-Sanchez, C.; Fernandez, V. M.; Pacheco, I.; Pereira, I. A. FTIR
40 Spectroelectrochemical Characterization of the Ni-Fe-Se Hydrogenase from *Desulfovibrio*
41 *vulgaris* Hildenborough. *J Biol Inorg Chem* **2008**, *13*, 1315-1320.
- 42
- 43 14. Parkin, A.; Goldet, G.; Cavazza, C.; Fontecilla-Camps, J. C.; Armstrong, F. A. The
44 Difference a Se Makes? Oxygen-Tolerant Hydrogen Production by the [NiFeSe]-Hydrogenase
45 from *Desulfomicrobium baculatum*. *J. Am. Chem. Soc.* **2008**, *130*, 13410-13416.
- 46
- 47 15. Wombwell, C.; Caputo, C. A.; Reisner, E. [NiFeSe]-Hydrogenase Chemistry. *Acc. Chem.*
48 *Res* **2015**, *48*, 2858-2865.
- 49
- 50
- 51 16. Garcin, E.; Vernede, X.; Hatchikian, E.; Volbeda, A.; Frey, M.; Fontecilla-Camps, J. The
52 Crystal Structure of a Reduced [NiFeSe] Hydrogenase Provides an Image of the Activated
53 Catalytic Center. *Structure* **1999**, *7*, 557-566.
- 54
- 55
- 56
- 57
- 58
- 59
- 60

- 1
2
3 17. Reich, H. J.; Hondal, R. J. Why Nature Chose Selenium. *ACS Chem. Biol.* **2016**, *11*, 821-
4 841.
5
6 18. Wombwell, C.; Reisner, E. Synthesis, Structure and Reactivity of Ni Site Models of
7 [NiFeSe] Hydrogenases. *Dalton Trans* **2014**, *43*, 4483-4493.
8
9 19. a) Wombwell, C.; Reisner, E. Synthetic Active Site Model of the [NiFeSe] Hydrogenase.
10 *Chem. Eur. J.* **2015**, *21*, 8096-8104. b) Marques, M.C.; Coelho, R.; Pereira I.A.C.; Matias, P.M.
11 Redox State-dependent Changes in the Crystal Structure of [NiFeSe] Hydrogenase from
12 *Desulfovibrio vulgaris Hildenborough*. *J. Mol. Biol.* **2010**, *396*, 893-907.
13
14 20. Volbeda, A.; Martin, L.; Cavazza, C.; Matho, M.; Faber, B. W.; Roseboom, W.; Albracht, S.
15 P. J.; Garcin, E.; Rousset, M.; Fontecilla-Camps, J. C. Structural Differences between the Ready
16 and Unready Oxidized States of [NiFe] hydrogenases. *J. Biol. Inorg. Chem.* **2005**, *10*, 239-249.
17
18 21. Cracknell J. A.; Wait A.F.; Lenz, O.; Friedrich, B; Armstrong, F. A. A Kinetic and
19 Thermodynamic Understanding of O₂ Tolerance in [NiFe]-hydrogenases. *Proc. Natl. Acad. Sci. U.*
20 *S. A.* **2009**, *106*, 20681-20686.
21
22 22. Jones, A. K.; Lamle, S. E.; Pershad, H. R.; Vincent, K. A.; Albracht, S. P. J.; Armstrong, F. A.
23 Enzyme Electrokinetics: Electrochemical Studies of the Anaerobic Interconversions between
24 Active and Inactive States of *Allochromatium vinosum* [NiFe]-hydrogenase. *J. Am. Chem. Soc.*
25 **2003**, *125*, 8505-8514.
26
27 23. Lamle, S. E.; Albracht, S. P.; Armstrong, F. A. The Mechanism of Activation of a [NiFe]-
28 Hydrogenase by Electrons, Hydrogen, and Carbon Monoxide. *J. Am. Chem. Soc.* **2005**, *127*,
29 6595-6604.
30
31 24. Radu, V.; Frielingsdorf, S.; Lenz, O.; Jeuken, L. J. Reactivation from the Ni-B State in
32 [NiFe] Hydrogenase of *Ralstonia eutropha* is Controlled by Reduction of the Superoxidised
33 Proximal Cluster. *Chem Commun* **2016**, *52*, 2632-2635.
34
35 25. Armstrong, F. A.; Belsey, N. A.; Cracknell, J. A.; Goldet, G.; Parkin, A.; Reisner, E.; Vincent,
36 K. A.; Wait, A. F. Dynamic Electrochemical Investigations of Hydrogen Oxidation and Production
37 by Enzymes and Implications for Future Technology. *Chem Soc Rev* **2009**, *38*, 36-51.
38
39 26. Albracht, S. P. J.; Graf, E. G.; Thauer, R. K. The EPR Properties of Nickel in Hydrogenase
40 from *Methanobacterium thermoautotrophicum*. *FEBS Lett.* **1982**, *140*, 311-313.
41
42 27. Flores, M.; Agrawal, A. G.; Gastel, V. M.; Gartner, W.; Lubitz, W. Electron-Electron
43 Double Resonance-Detected NMR to Measure Metal Hyperfine Interactions: ⁶¹Ni in the Ni-B
44 State of the [NiFe] Hydrogenase of *Desulfovibrio Vulgaris* Miyazaki F. *J. Am. Chem. Soc.* **2008**,
45 *130*, 2402-2403.
46
47 28. Horch, M.; Lauterbach, L.; Mroginski, M. A.; Hildebrandt, P.; Lenz, O.; Zebger, I.
48 Reversible Active Site Sulfoxylation Can Explain the Oxygen Tolerance of a NAD⁺-Reducing
49 [NiFe] Hydrogenase and Its Unusual Infrared Spectroscopic Properties. *J. Am. Chem. Soc.* **2015**,
50 *137*, 2555-2564.
51
52
53
54
55
56
57
58
59
60

- 1
2
3 29. Volbeda, A.; Martin, L.; Barbier, E.; Gutierrez-Sanz, O.; DeLacey, A. L.; Liebgott, P.;
4 Dementin, S.; Rousset, M.; Fontecilla-Camps, J. C. Crystallographic Studies of [NiFe]-
5 hydrogenase Mutants: towards Consensus Structures for the Elusive Unready Oxidized States. *J.*
6 *Biol. Inorg. Chem.* **2014**, *20*, 11-22.
- 7
8 30. Marques, M. C.; Coelho, R.; De Lacey, A. L.; Pereira, I. A. C.; Matias, P. M. The Three-
9 Dimensional Structure of [NiFeSe] Hydrogenase from *Desulfovibrio vulgaris* Hildenborough: A
10 Hydrogenase without a Bridging Ligand in the Active Site in Its Oxidised, "as-Isolated" State. *J*
11 *Mol Biol* **2010**, *396*, 893-907.
- 12
13 31. Volbeda, A.; Amara, P.; Iannello, M.; De Lacey, A. L.; Cavazza, C.; Fontecilla-Camps, J. C.
14 Structural Foundations for the O₂ Resistance of *Desulfomicrobium baculatum* [NiFeSe]-
15 hydrogenase. *Chem Commun* **2013**, *49*, 7061-7063.
- 16
17 32. Teixeira, M.; Fauque, G.; Moura, I.; Lespinat, P. A.; Berlier, Y.; Prickril, B.; Peck H. D.;
18 Xavier, A. V.; Gall, J. L.; Moura, J. J. G. Nickel-[iron-sulfur]-selenium-containing Hydrogenases
19 from *Desulfovibrio baculatus* (DSM 1743). *Eur. J. Biochem.* **1987**, *167*, 47-58.
- 20
21 33. Marques, M. C.; Tapia, C.; Gutierrez-Sanz, O.; Ramos, A. R.; Keller, K. L.; Wall, J. D.; De
22 Lacey, A. L.; Matias, P. M.; Pereira, I. A. C. The Direct Role of Selenocysteine in [NiFeSe]
23 Hydrogenase Muturation and Catalysis. *Nat. Chem. Biol.* **2017**, *13*, 544-550.
- 24
25 34. Grapperhaus, C. A.; Maguire, M. J.; Tuntulani, T.; Darensbourg, M. Y. Singlet Oxygen and
26 the Production of Sulfur Oxygenates of Nickel(II) and Palladium(II) Thiolates. **1997**, *36*, 1860-
27 1866.
- 28
29 35. Farmer, P. J.; Solouki, T.; Mills, D. K.; Soma, T.; Russell, D. H.; Reibenspies, J. H.;
30 Darensbourg, M. Y. Isotopic Labeling Investigation of Oxygenation of Nickel-Bound Thiolates by
31 Molecular Oxygen. *J. Am. Chem. Soc.* **1992**, *114*, 4601-4605.
- 32
33 36. Grapperhaus, C. A.; Darensbourg, M. Y. Oxygen Capture by Sulfur in Nickel Thiolates. *Acc.*
34 *Chem. Res.* **1998**, *31*, 451-459.
- 35
36 37. Grapperhaus, C. A.; Darensbourg, M. Y.; Sumner, L. W.; Russell, D. H. Template Effect for
37 O₂ Addition across cis-Sulfur Sites in Nickel Dithiolates. *J. Am. Chem. Soc.* **1996**, *118*, 1791-1792.
- 38
39 38. Farmer, P.J.; Solouki, T.; Soma, T.; Russell, D.H.; Darensbourg, M. Y. Divergent Pathways
40 for the Addition of Dioxygen to Sulfur in Nickel cis-Dithiolates: An Isotopomeric Analysis. *Inorg.*
41 *Chem.* **1993**, *32*, 4171-4172.
- 42
43 39. Lindenmaier, N. J.; Wahlefeld, S.; Bill, E.; Szilvasi, T.; Eberle, C.; Yao, S.; Hildebrandt, P.;
44 Horch, M.; Zebger, I.; Driess, M. An S-oxygenated [NiFe] Complex Modelling Sulfenate
45 Intermediates of an O₂-Tolerant Hydrogenase. *Angew. Chem. Int. Ed.* **2017**, *56*, 2208-2211.
- 46
47 40. Choudhury, S. B.; Pressler, M. A.; Mirza, S. A.; Day, R. O.; Maroney, M. J. Structure and
48 Redox Chemistry of Analogous Nickel Thiolato and Selenolato Complexes: Implications for the
49 Nickel Sites in Hydrogenase. *Inorg. Chem.* **1994**, *33*, 4831-4839.
- 50
51
52
53
54
55
56
57
58
59
60

- 1
2
3 41. Yang, X.; Elrod, L. C.; Reibenspies, J. H.; Hall, M. B.; Darensbourg, M. Y. Oxygen Uptake in
4 Complexes Related to [NiFeS]- and [NiFeSe]- hydrogenase Active Sites. *Chem. Sci.* **2019**, *10*,
5 1368-1373.
6
7 42. Broering, E. P.; Dillon, S.; Gale, E. M.; Steiner, R. A.; Telsler, J.; Brunold, T. C.; Harrop, T. C.
8 Accessing Ni(III)-Thiolate Versus Ni(II)-Thiyl Bonding in a Family of Ni-N₂S₂ Synthetic Models of
9 NiSOD. *Inorg. Chem.* **2015**, *54*, 3815-3828.
10
11 43. Jenkins, R. M.; Singleton, M. L.; Leamer, L. A.; Reibenspies, J. H.; Darensbourg, M. Y.
12 Orientation and Stereodynamic Paths of Planar Monodentate Ligands in Square Planar Nickel
13 N₂S complexes. *Inorg. Chem.* **2010**, *49*, 5503-5514.
14
15 44. Hammett, L. P. The Effect of Structure upon the Reactions of Organic Compounds
16 Benzene Derivatives. *J. Am. Chem. Soc.* **1937**, *59*, 96-103.
17
18 45. Gaussian 16, R. B., M. J. Frisch, G. W. Trucks, H. B. Schlegel, G. E. Scuseria, M. A. Robb, J.
19 R. Cheeseman, G. Scalmani, V. Barone, G. A. Petersson, H. Nakatsuji, X. Li, M. Caricato, A. V.
20 Marenich, J. Bloino, B. G. Janesko, R. Gomperts, B. Mennucci, H. P. Hratchian, J. V. Ortiz, A. F.
21 Izmaylov, J. L. Sonnenberg, D. Williams-Young, F. Ding, F. Lipparini, F. Egidi, J. Goings, B. Peng, A.
22 Petrone, T. Henderson, D. Ranasinghe, V. G. Zakrzewski, J. Gao, N. Rega, G. Zheng, W. Liang, M.
23 Hada, M. Ehara, K. Toyota, R. Fukuda, J. Hasegawa, M. Ishida, T. Nakajima, Y. Honda, O. Kitao,
24 H. Nakai, T. Vreven, K. Throssell, J. A. Montgomery, Jr., J. E. Peralta, F. Ogliaro, M. J. Bearpark, J.
25 J. Heyd, E. N. Brothers, K. N. Kudin, V. N. Staroverov, T. A. Keith, R. Kobayashi, J. Normand, K.
26 Raghavachari, A. P. Rendell, J. C. Burant, S. S. Iyengar, J. Tomasi, M. Cossi, J. M. Millam, M.
27 Klene, C. Adamo, R. Cammi, J. W. Ochterski, R. L. Martin, K. Morokuma, O. Farkas, J. B.
28 Foresman, and D. J. Fox, Gaussian, Inc., Wallingford CT, 2016.
29
30 46. AMPAC 9 (Semichem Inc., S., KS, 2008).
31
32 47. Glendening E.D., B. J. K., Reed A. E., Carpenter J. E., Bohmann J. A., Morales C. M., Landis
33 C. R. and Weinhold F., (2013), NBO 6.0. Theoretical Chemistry Institute, University of Wisconsin:
34 Madison, WI.
35
36 48. Isegawa, M.; Sharma, A. K.; Ogo, S.; Morokuma, K. DFT Study on Fe(IV)-Peroxo
37 Formation and H Atom Transfer Triggered O₂ Activation by NiFe Complex. *Organometallics*
38 **2018**, *37*, 1534-1545.
39
40 49. Ogo, S. H₂ and O₂ Activation- A Remarkable Insight into Hydrogenase. *Chem. Rec.* **2014**,
41 *14*, 397-409.
42
43 50. Ogo, S. H₂ and O₂ Activation by [NiFe]hydrogenase -Insights from model complexes.
44 *Coord. Chem. Rev.* **2017**, *334*, 43-53.
45
46 51. Westheimer, F. H. Why Nature Chose Phosphates. *Science* **1987**, *235*, 1173-1178.
47
48 52. Lauterbach, L.; Lenz, O. Catalytic Production of Hydrogen Peroxide and Water by
49 Oxygen-Tolerant [NiFe]-Hydrogenase during H₂ Cycling in the Presence of O₂. *J. Am. Chem. Soc.*
50 **2013**, *135*, 17897-17905.
51
52
53
54
55
56
57
58
59
60

1
2
3
4
5
6
7
8
9
10
11
12
13
14
15
16
17
18
19
20
21
22
23
24
25
26
27
28
29
30
31
32
33
34
35
36
37
38
39
40
41
42
43
44
45
46
47
48
49
50
51
52
53
54
55
56
57
58
59
60

TOC graphic:

